Solar Energy Materials & Solar Cells 94 (2010) 478–483

Contents lists available at ScienceDirect

Solar Energy Materials & Solar Cells

journal homepage: www.elsevier.com/locate/solmat

# Finite element simulations of compositionally graded InGaN solar cells

G.F. Brown [a,b,*], J.W. Ager III[b], W. Walukiewicz [b], J. Wu [a,b]

[a] Department of Materials Science & Engineering, University of California, Berkeley, California 94720, USA
[b] Materials Sciences Division, Lawrence Berkeley National Laboratory, Berkeley, California 94720, USA

ARTICLE INFO

*Article history:*
Received 22 May 2008
Received in revised form
5 November 2009
Accepted 9 November 2009
Available online 27 November 2009

*Keywords:*
Device modeling
InGaN
Composition grading
Heterojunction

ABSTRACT

The solar power conversion efficiency of compositionally graded $In_xGa_{1-x}N$ solar cells was simulated using a finite element approach. Incorporating a compositionally graded region on the InGaN side of a p-GaN/n-$In_xGa_{1-x}N$ heterojunction removes a barrier for hole transport into GaN and increases the cell efficiency. The design also avoids many of the problems found to date in homojunction cells as no p-type high-In content region is required. Simulations predict 28.9% efficiency for a p-GaN/n-$In_xGa_{1-x}N$/n-$In_{0.5}Ga_{0.5}N$/p-Si/n-Si tandem structure using realistic material parameters. The thickness and doping concentration of the graded region was found to substantially affect the performance of the cells.



## 1. Introduction

$In_xGa_{1-x}N$ alloys feature a bandgap ranging from the near infrared (0.7 eV) to the ultraviolet (3.4 eV) [1,2]. This range corresponds very closely to the solar spectrum making $In_xGa_{1-x}N$ alloys a promising candidate for radiation-resistant multi-junction solar cells [3]. Furthermore, it has been shown that $In_xGa_{1-x}N$ can be grown directly on Si substrates by a low temperature process, providing the potential for cheap multi-junction solar cells [4]. Previous simulations have shown that double-junction $In_xGa_{1-x}N$/Si cells could have efficiencies as high as 31% [5].

$In_xGa_{1-x}N$ solar cells have been fabricated by a number of groups although only for Indium compositions less than 30% [6–9]. One of the main challenges towards increasing the Indium content in these cells is p-type doping. P-type doping has only recently been established for InN and has been verified by electrochemical capacitance voltage measurements [10], variable magnetic field Hall effect [11] and thermopower [12]. The difficulty in doping InN p-type is believed to come from compensation by native defects. The Fermi-stabilization level [13] lies above the conduction band of $In_xGa_{1-x}N$ for Indium compositions greater than ~40%, causing native defects in $In_xGa_{1-x}N$ to act as donors which pin the surface Fermi level in the conduction band [14]. In addition, in p-type $In_xGa_{1-x}N$ with $x > 60\%$, a surface inversion layer forms preventing direct contact to the p-type bulk [15,16]. These difficulties limit the range of compositions available for fabricating solar cells.

One method around these problems is to use p-GaN/n-$In_xGa_{1-x}N$ heterojunctions instead of a homojunction [6,8,9,17]. In this design, a highly conductive p-type GaN layer provides the hole contact while absorption takes place in the lower bandgap $In_xGa_{1-x}N$ layer. Furthermore, the GaN functions as a natural window layer reducing surface recombination. Highly conductive p-type GaN layers with resistivities lower than 1.3 Ω cm have recently been grown, which could provide a low-resistance window layer [18]. However, as will be shown in this paper, a p-GaN/n-$In_xGa_{1-x}N$ heterojunction has a valence band discontinuity that increases with Indium content. This discontinuity restricts photo-generated holes from crossing the heterojunction, lowering the device efficiency.

In this paper, we evaluate the effect of inserting a graded $In_xGa_{1-x}N$ region between a p-GaN/n-$In_xGa_{1-x}N$ heterojunction. Compositional grading has been shown experimentally to remove band discontinuities at heterointerfaces [19]. The design is technologically feasible, as it has been shown that graded $In_xGa_{1-x}N$ layers can be grown over the entire composition range using the Energetic Neutral Atom Beam Lithography and Epitaxy (ENABLE) process [20]. Compositional grading in solar cells has previously been considered in the $Al_xGa_{1-x}As$ materials system, where it was found to reduce surface recombination losses [21,22]. Grading has also been used in $CuIn_xGa_{1-x}Se_2$ cells to increase the efficiencies in thin devices [23]. However, the design considered in this paper differs as the graded layer is confined within the depletion region in order to remove the valence band

* Corresponding author at: University of California Department of Materials Science & Engineering 210 Hearst Memorial Mining Building Rm 114 Berkeley, CA 94720, USA. Tel.: +1 415 279 3468.
*E-mail address:* gregory.f.brown@gmail.com (G.F. Brown).

0927-0248/$ - see front matter © 2009 Elsevier B.V. All rights reserved.
doi:10.1016/j.solmat.2009.11.010

discontinuity. We show that incorporating graded layers of $In_xGa_{1-x}N$ into devices allows the production of efficient high Indium content solar cells.

## 2. Properties of $In_xGa_{1-x}N$ used in simulations

The dielectric constant ($\varepsilon_s$), electron effective mass ($m_e$), hole effective mass ($m_h$), bandgap ($E_g$), electron affinity ($E_a$), minority electron lifetime ($\tau_e$) and minority hole lifetime ($\tau_h$) parameters used in the simulation are summarized in Table 1. For a p-GaN/n-$In_xGa_{1-x}N$ heterojunction solar cell, the minority hole lifetime strongly affects the overall efficiency since most of the light absorption occurs in the n-type layer. Hole lifetimes as high as 6.5 and 5.4 ns have been observed in GaN and InN [31,32]. However, $In_xGa_{1-x}N$ alloys are likely to have lower lifetimes due to compositional fluctuations, and therefore a 1 ns minority hole lifetime was assumed.

The electron and hole mobilities were calculated as a function of doping using [29]:

$$\mu_i(N) = \mu_{\min,i} + \frac{\mu_{\max,i} - \mu_{\min,i}}{1 + (N/N_{g,i})^{\gamma_i}}, \quad (1)$$

where $i$ represents either electrons ($e$) or holes ($h$), $N$ is the doping concentration and $\mu_{\min}$, $\mu_{\max}$, $\gamma$ and $N_g$ are parameters specific to a given semiconductor [29]. The values used in the simulations are given in Table 1. $In_xGa_{1-x}N$ electron mobilities were taken as a linear interpolation between the GaN and InN values. This approach ignores the effects of alloy disorder scattering, which reduces the electron mobility. However, as most of the incident light will be absorbed in the n-type region, the electron mobility will not strongly affect the simulation results.

In the absence of experimental data on hole mobilities in $In_xGa_{1-x}N$ alloys, the maximum InN hole mobility was assumed to be twice that of GaN, based on the assumption that the hole effective mass in InN is half that of GaN. Once again, this approach ignores the effect of alloy scattering, which would reduce the hole mobility. The hole mobility, along with the minority carrier lifetime, will determine the minority carrier diffusion length which in turns affects the device efficiency.

Wavelength-dependant absorption coefficients for $In_xGa_{1-x}N$ alloys were taken from literature for Indium compositions of 1, 0.83, 0.69, 0.57, 0.5 and 0 [1,33]. The data was then fit to the equation

$$\alpha(E) = 10^5 \sqrt{a\cdot(E-E_g) + b\cdot(E-E_g)^2}\,\mathrm{cm}^{-1}, \quad (2)$$

where $E$ is the incoming photon energy given in eV and $a$ and $b$ are dimensionless fitting parameters. The fitting parameters used in the simulation are shown in Table 2. A linear interpolation was used to find the fitting parameters over the entire composition range. In this manner, the wavelength-dependant absorption coefficient was determined for all alloy compositions. This allows the absorption coefficient to vary in each layer of the simulated device based on the local Gallium concentration.

**Table 1**
Properties of GaN and InN used in the simulations. The note describes whether the $In_xGa_{1-x}N$ alloy properties were determined using a linear interpolation or if a bowing parameter was used. The mobility model is described by Eq. 1 in the text.

| Property | GaN | InN | Note |
|---|---|---|---|
| $\varepsilon_s/\varepsilon_0$ | 8.9 [24] | 10.5 [25] | Linear interpolation |
| $m_e/m_0$ | 0.2 [24] | 0.05 [26] | Linear interpolation |
| $m_h/m_0$ | 1.25 [27] | 0.6[a] | Linear interpolation |
| $E_g$ (eV) | 3.42 [2,28] | 0.7 [2,28] | 1.43 bowing |
| $E_a$ (eV) | 4 [2,28] | 5.6 [2,28] | 0.8 bowing |
| $\tau_e$ (ns) | 1 | 1 | |
| $\tau_h$ (ns) | 1 | 1 | |
| $\mu_{\min,e}$ ($cm^2V^{-1}s^{-1}$) | 55 [29] | 30 [30] | |
| $\mu_{\max,e}$ ($cm^2V^{-1}s^{-1}$) | 1000 [29] | 1100 [30] | |
| $\gamma_e$ | 1 [29] | 1 [30] | |
| $N_{g,e}$ ($cm^{-3}$) | $2\times10^{17}$ [29] | $8\times10^{18}$[30] | |
| $\mu_{\min,h}$ ($cm^2V^{-1}s^{-1}$) | 3 [29] | 3 | |
| $\mu_{\max,h}$ ($cm^2V^{-1}s^{-1}$) | 170 [29] | 340[b] | |
| $\gamma_h$ | 2 [29] | 2 | |
| $N_{g,h}$ ($cm^{-3}$) | $3\times10^{17}$ [29] | $3\times10^{17}$ | |

[a] Little experimental data is available for the hole effective mass so a value of 0.6 was used.
[b] The maximum hole mobility was assumed to be twice that of GaN, based on the estimated effective hole mass of InN being half the value of GaN.

**Table 2**
Fitting parameters used to calculate the absorption coefficient of $In_xGa_{1-x}N$ alloys.

| Indium composition | a | b |
|---|---|---|
| 1 | 0.69642 | 0.46055 |
| 0.83 | 0.66796 | 0.68886 |
| 0.69 | 0.58108 | 0.66902 |
| 0.57 | 0.60946 | 0.62182 |
| 0.5 | 0.51672 | 0.46836 |
| 0 | 3.52517 | −0.65710 |

## 3. Simulation results

The semiconductor finite element analysis software APSYS was used to simulate the InGaN heterojunction solar cells. The software self-consistently solves the Poisson and carrier drift-diffusion equations, and allows for compositionally dependant material parameters. Some assumptions were used to reduce the number of adjustable material parameters. First, InGaN has the wurtzite crystal structure and therefore both piezoelectric and spontaneous polarization, which can affect the charge distribution within each layer [17,34]. These effects were not included as it is difficult to make general statements about the strain in each layer, particularly when graded layers are used. Second, the Fermi level at the InGaN/GaN interface was assumed to be un-pinned. While there is no experimental evidence of pinning at this interface, several studies have shown surface states lead to surface inversion layers in p-type $In_xGa_{1-x}N$ ($x > 0.49$) [16]. Therefore, interface defects could also pin the interface Fermi level. Reflection and light trapping effects were also not included in the simulation. Reflection losses would serve to reduce the overall efficiency while light trapping would increase the efficiency by increasing the absorption probability for the light entering the cell. Surface recombination losses were also not considered, although they are likely to be low as the p-GaN top layer is used as a window layer. Fig. 1 illustrates this by showing the optical carrier generation as a function of depth through a GaN/$In_{0.5}Ga_{0.5}N$ heterojunction where the top layer is 100 nm and the bottom layer is 1 μm. Very few carriers are generated in the top 100 nm of GaN, as a low percentage of the AM 1.5 spectrum is above the bandgap of GaN. This is beneficial as the minority carrier properties of the GaN can be poor without affecting the solar cell efficiency.

Fig. 2 shows the calculated band diagram and $I$–$V$ curve for a p-GaN/n-$In_{0.5}Ga_{0.5}N$ ($E_g$=1.7 eV) structure. This particular bandgap would be well suited for a high-efficiency InGaN/Si double-junction cell [5]. However, a sharp valence band offset can be seen at the interface between the two layers. This valence band offset prevents minority holes generated in the $In_{0.5}Ga_{0.5}N$ layer from crossing into the p-GaN layer. Therefore, the current generated in such a structure only comes from the absorption in the GaN layer.

This leads to a very small short-circuit current and an AM 1.5 efficiency of 0.35%.

Fig. 3 shows the efficiency, short-circuit current and fill factor as a function of Indium composition for the p-GaN/n-$In_xGa_{1-x}N$ structure. Initially, the increase in Indium composition leads to a higher short-circuit current and efficiency due to the decreasing bandgap of the absorbing layer. The efficiency peaks at 13.4% at a composition of roughly $In_{0.35}Ga_{0.65}N$, after which it falls steeply as the valence band discontinuity becomes too large for minority hole collection. The band diagram for a GaN/$In_{0.35}Ga_{0.65}N$ cell looks very similar to that in Fig. 2 except the valence band discontinuity is smaller. For Indium concentrations above 50%, the discontinuity is too severe for minority holes to overcome and all of the electron-hole pairs generated in this layer are lost to recombination. The rapid drop in short-circuit current in this composition range stems from the valence band discontinuity blocking the collection of minority holes generated in the InGaN layer. At roughly the same Indium composition, the fill factor exhibits a sharp dip due to the increasing series resistance of the cell which is a result of the valence band discontinuity. The fill factor then rises back to its original value, as the only contribution to the photocurrent comes from minority electrons in the p-GaN layer. The efficiency and short-circuit current for this structure are roughly constant above 50% Indium.

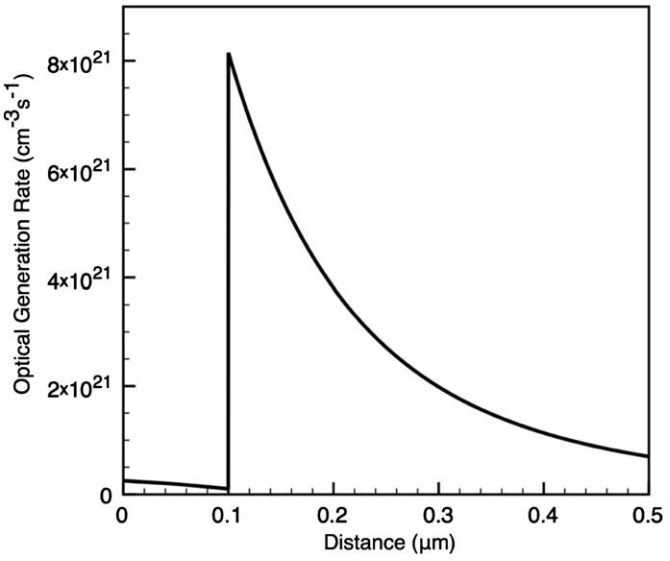


**Fig. 1.** Optical carrier generation rate as a function of distance through a p-GaN/n-$In_{0.5}Ga_{0.5}N$ cell under AM 1.5 illumination. The GaN ($In_{0.5}Ga_{0.5}N$) layer is 100 nm (1 μm) thick.

The composition at which the valence band discontinuity affects minority carrier collection is determined primarily by the choice of valence band offset between InN and GaN. A wide range of values from 0.5 eV [35] to 1.1 eV [36] have been determined from experimental and theoretical approaches making it difficult to pinpoint the composition at which this effect will dominate the *I–V* characteristics [2]. If the valence band offset is significantly smaller than 1.1 eV (the value used in this paper), a higher Indium composition could be incorporated into the heterojunction design.

To remove the valence band discontinuity, a graded n-$In_xGa_{1-x}N$ region was inserted between the p-GaN and n-$In_{0.5}Ga_{0.5}N$ layers. The graded layer is incorporated into the simulation as 40 discrete layers with a linear change in Gallium composition between each layer. Fig. 4 shows the band diagram of a p-GaN/n-$In_xGa_{1-x}N$/$In_{0.5}Ga_{0.5}N$ structure. The top, middle and back layers are 100 nm, 50 nm and 1 μm thick, respectively. The doping concentration in the n-type layer is $1\times10^{17}$ and $5\times10^{18}$ cm$^{-3}$ in the p-type layer. The valence band discontinuity

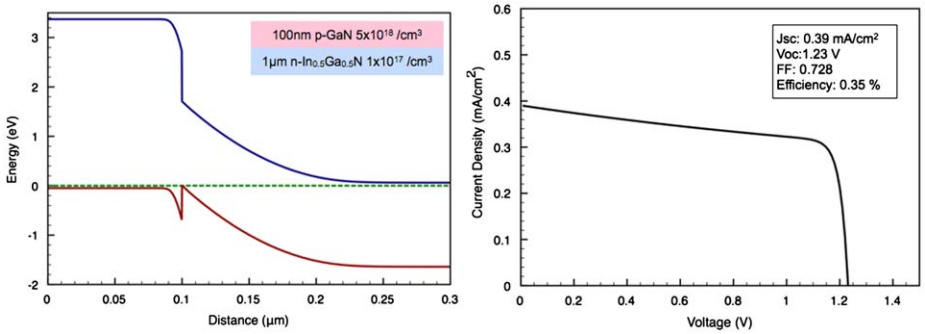


**Fig. 2.** (Left) Band diagram of a p-GaN/n-$In_{0.5}Ga_{0.5}N$ structure (first 300 nm shown) under zero bias. (Right) *I–V* curve for the structure under AM 1.5 illumination. The photo-generated current originates solely from the p-GaN layer.

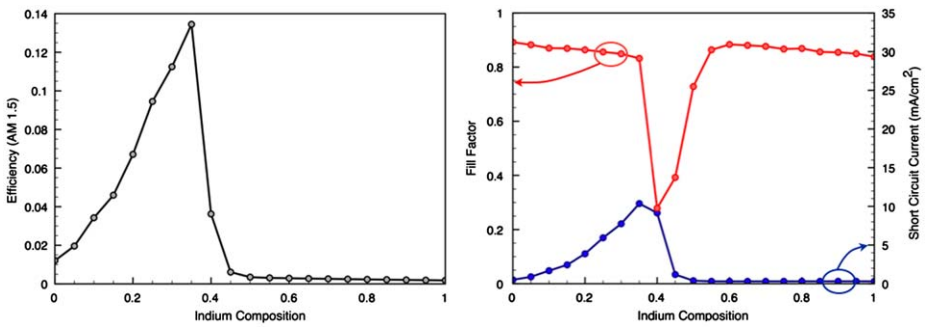


**Fig. 3.** (Left) Calculated AM 1.5 efficiency of a single-junction p-GaN/n-$In_xGa_{1-x}N$ structure versus Indium composition. The structure is the same as given in Fig. 2. (Right) Fill factor and short-circuit current versus Indium composition.

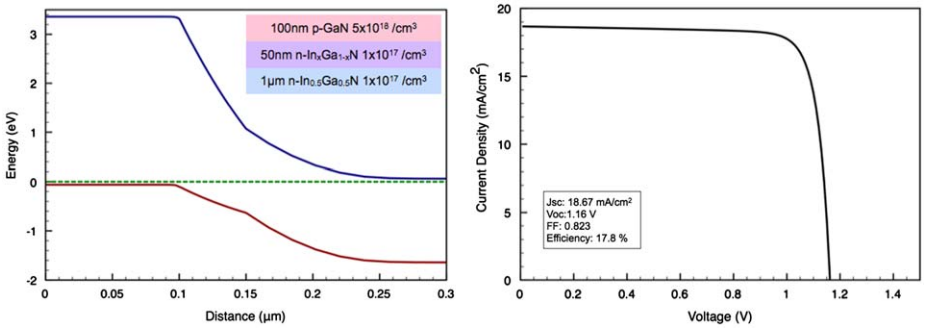


**Fig. 4.** (Left) Band diagram of p-GaN/n-$In_xGa_{1-x}N$/n-$In_{0.5}Ga_{0.5}N$ structure (first 300 nm shown). The middle layer is graded from GaN at the top to $In_{0.5}Ga_{0.5}N$ at the bottom. (Right) *I–V* curve for the structure under AM 1.5 illumination.

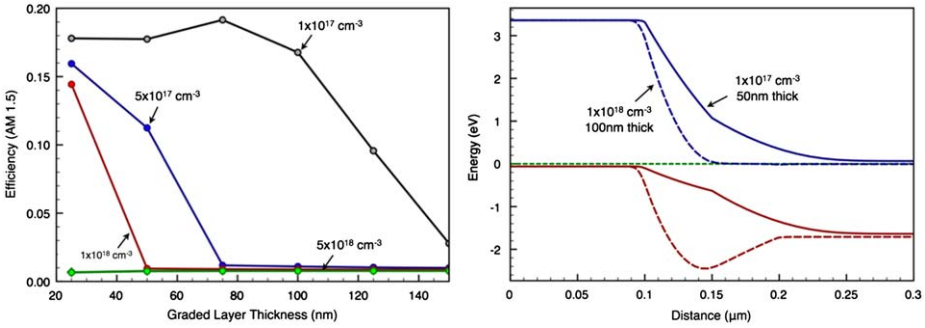


**Fig. 5.** (Left) Efficiency of graded p-GaN/n-$In_xGa_{1-x}N$/n-$In_{0.5}Ga_{0.5}N$ structures as a function of the graded layer thickness. Four different n-type doping levels are considered. The top GaN layer is 100 nm and the bottom $In_{0.5}Ga_{0.5}N$ layer is 1 μm thick. (Right) Band diagrams showing that a lightly doped thin graded region effectively removes the valence band offset, but a heavily doped thick graded region introduces an electric field opposing minority hole collection (first 300 nm shown). This electric field opposing minority hole collection is responsible for the decrease in efficiency with increasing layer thickness and doping.

present in Fig. 2 has been replaced with a smooth transition from the Indium-rich to Gallium-rich side. Fig. 4 also shows the simulated *I–V* curve for such a structure exhibiting a short-circuit current of 18.7 mA/cm$^2$, roughly 50 times higher than the ungraded structure in Fig. 2. The large increase in current is due to the removal of the valence band discontinuity, which increases the collection efficiency in the $In_{0.5}Ga_{0.5}N$. The corresponding AM 1.5 efficiency for this structure is 17.8%.

One of the most critical design aspects is the doping and thickness of the graded $In_xGa_{1-x}N$ layer. Fig. 5 shows the change in efficiency as a function of n-type doping concentration and graded layer thickness. The highest efficiencies are achieved for thin layers with low doping. Increasing the thickness of the graded layer beyond the depletion region generates a quasi-electric field that opposes minority carrier collection. Similarly, increasing the doping of the graded layer decreases the depletion region thickness and requires a much thinner graded layer to achieve high efficiencies. Fig. 5 shows the band diagrams for two structures representing a lightly doped thin layer and a heavily doped, thick layer. In the case of the highly doped thick layer, the grading introduces a barrier preventing photo-generated holes from being collected.

Confining the graded layer within the depletion region is therefore required for high-efficiency devices. However, this limitation could be overcome by making the graded region p-type. In this case, the electric field generated within the graded region would actually improve minority carrier collection. However, this design may prove difficult in practice due to the previously discussed difficulty in doping Indium rich alloys p-type. Instead, it may be more realistic to focus on lowering the background electron concentration in the graded layer. This too is non-trivial due to the aforementioned propensity for n-type doping in Indium-rich InGaN. Furthermore, if the interface Fermi level were pinned close to the InGaN conduction band, the depletion width would be decreased making it more difficult to confine the grading-induced electric field.

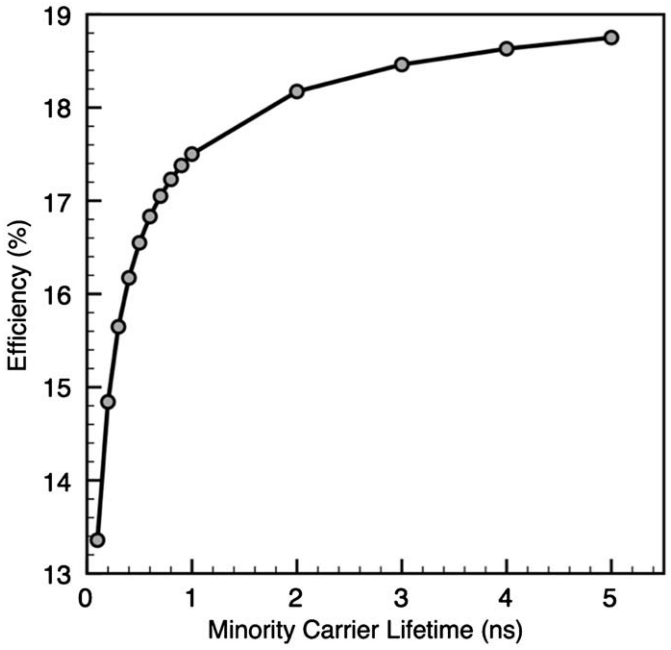


**Fig. 6.** Efficiency of a graded p-GaN/n-$In_xGa_{1-x}N$/n-$In_{0.5}Ga_{0.5}N$ structure versus minority hole lifetime in the InGaN layer. The graded region is 50 nm thick with a doping concentration of $10^{17}$ cm$^{-3}$. The top GaN layer is 100 nm and the bottom $In_{0.5}Ga_{0.5}N$ layer is 1 μm thick.

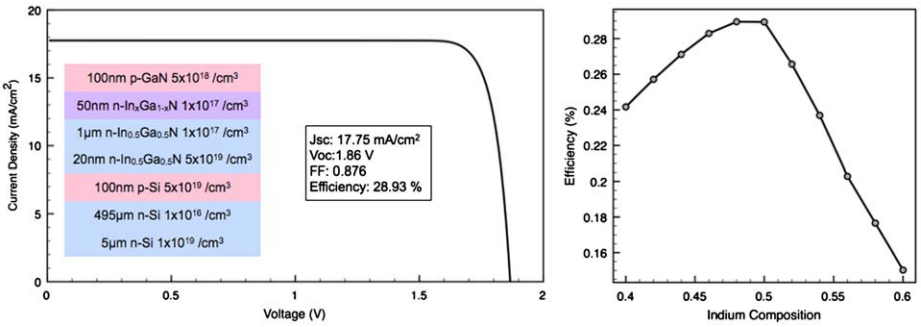


**Fig. 7.** (Left) *I–V* curve for a graded p-GaN/n-$In_xGa_{1-x}N$/n-$In_{0.5}Ga_{0.5}N$/p-Si/n-Si structure. (Right) Efficiency versus Indium composition of the top cell. The maximum efficiency is roughly 28.9% at $In_{0.5}Ga_{0.5}N$, corresponding to a top bandgap of 1.7 eV.

The minority carrier lifetime is one of the most critical parameters in determining the efficiency of a solar cell. As discussed previously, experimental data for minority carrier lifetimes does not exist across the composition range for $In_xGa_{1-x}N$. Therefore, we simulated the effect that lower lifetimes would have on device performance. Fig. 6 shows the effect of minority carrier lifetime on cell efficiency. The large absorption coefficient in the direct-bandgap $In_xGa_{1-x}N$ causes the majority of electron-hole pairs to be generated less than a diffusion length away from the junction even for short minority carrier lifetimes. It should be noted that the minority carrier diffusion length also depends on the mobility of the carriers, therefore estimation in these values leads to uncertainty in the simulation results.

One of the most promising applications for these graded InGaN cells is in tandem cells. The tunability of the bandgap across the entire solar spectrum allows for multiple InGaN cells to be stacked on top of one another to increase device efficiencies [3,5]. Alternatively, InGaN can be grown directly on Si substrates opening up the possibility for highly efficient, inexpensive double-junction cells. An InGaN/Si tandem cell would have the additional benefit of a natural tunnel junction between the p-Si and n-InGaN, thereby eliminating the need for highly doped regions in conventional multi-junction solar cells [4,5].

Fig. 7 shows the *I–V* curve for an InGaN/Si structure assuming a minority carrier lifetime of 1 ms for Si and an electron (hole) mobility of 130 (420) $cm^2\ V^{-1}\ sec^{-1}$. These values were chosen to represent high-quality Si. A simulated p-Si/n-Si cell using these parameters resulted in an efficiency of 22.5%, which is typical of high-efficiency Si cells [37]. Fig. 7 also shows how the composition of the top InGaN cell affects the efficiency of the entire device. A peak efficiency of 28.9% corresponds to an $In_{0.5}Ga_{0.5}N$ top cell where the photo-generated current in the InGaN and Si layer match each other. In this design, the graded InGaN layer again serves to eliminate the hole barrier and the need for p-type doping of InGaN.

The 28.9% peak efficiency for this simulated double-junction cell is comparable to high-efficiency InGaP/GaAs double-junction cells, which can exhibit efficiencies over 30% [38]. The slightly lower efficiency is due to a lower minority carrier diffusion length assumed in the modeling; however these InGaN cells have the benefit of utilizing Si as a cheaper substrate. Currently, p-GaN/n-$In_{0.12}Ga_{0.88}N$/n-GaN heterojunction cells have achieved internal quantum efficiencies close to 94%, further indicating high-efficiency InGaN cells are achievable [8]. It is likely that increasing the Indium content of the cells will also increase the dislocation density within the active region, however high-efficiency InGaN light-emitting diodes are achievable even when dislocation densities are orders of magnitude higher than comparable AlGaAs and AlInGaP devices [39].

## 4. Conclusions

Finite element simulations were used to simulate graded p-GaN/n-$In_xGa_{1-x}N$ heterojunctions. A graded layer inserted between the heterojunction was found to eliminate the valence band offset at the interface. The doping and width of the graded layer had a profound effect on device efficiencies, where lightly doped thin layers exhibited the highest efficiencies. Double-junction graded InGaN/Si cells were also simulated using realistic parameters resulting in device efficiencies above 28.9%. These cells offer the potential of high conversion efficiencies combined with low-cost substrates.

## Acknowledgements

This work was supported in part by National Science Foundation under Grant No. CBET-0932905, and a LDRD grant from the Lawrence Berkeley National Laboratory. JWA was supported by the Director, Office of Science, Office of Basic Energy Sciences, Materials Sciences and Engineering Division of the U.S. Department of Energy, Contract No. DE-AC02-05CH11231.

## References

[1] J. Wu, W. Walukiewicz, K.M. Yu, J.W. Ager III, E.E. Haller, H. Lu, W.J. Schaff, Small band gap bowing in $In_{1-x}Ga_xN$ alloys, Appl. Phys. Lett. 80 (2002) 4741–4743.
[2] J. Wu, When group III-nitrides go infrared: new properties and perspectives, J. Appl. Phys. 106 (2009) 011101-1–28.
[3] J. Wu, W. Walukiewicz, K.M. Yu, W. Shan, J.W. Ager III, E.E. Haller, H. Lu, W.J. Schaff, W.K. Metzger, S. Kurtz, Superior radiation resistance of $In_{1-x}Ga_xN$ alloys: Full-solar-spectrum photovoltaic material system, J. Appl. Phys. 94 (2003) 6477–6482.
[4] L.A. Reichertz, K.M. Yu, Y. Cui, M.E. Hawkridge, J.W. Beeman, Z. Liliental-Weber, J.W. Ager III, W. Walukiewicz, W.J. Schaff, T.L. Williamson, M.A. Hoffbauer, InGaN thin films grown by ENABLE and MBE techniques on silicon substrates, Mater. Res. Soc. Symp. Proc. 1068 (2008) C-06-02.
[5] L. Hsu, W. Walukiewicz, Modeling of InGaN/Si tandem solar cells, J. Appl. Phys. 104 (2008) 024507-1–7.
[6] O. Jani, I. Ferguson, C. Honsberg, S. Kurtz, Design and characterization of GaN/InGaN solar cells, Appl. Phys. Lett. 91 (2007) 132117-1–3.
[7] X. Chen, K.D. Matthews, D. Hao, W.J. Schaff, L.F. Eastman, Growth, fabrication, and characterization of InGaN solar cells, phys. Stat. sol. (a) 205 (2008) 1103–1105.
[8] C.J. Neufeld, N.G. Toledo, S.C. Cruz, M. Iza, S.P. DenBaars, W.K. Mishra, High quantum efficiency InGaN/GaN solar cells with 2.95 eV band gap, Appl. Phys. Lett. 93 (2008) 143502–1–3.
[9] X. Zheng, R. Horng, D. Wuu, M. Chu, W. Liao, M. Wu, R. Lin, Y. Lu, High-quality InGaN/GaN heterojunctions and their photovoltaic effects, Appl. Phys. Lett. 93 (2008) 261108-1–3.
[10] R.E. Jones, K.M. Yu, S.X. Li, W. Walukiewicz, J.W. Ager, E.E. Haller, H. Lu, W.J. Schaff, Evidence for p-Type Doping of InN, Phys. Rev. Lett. 96 (2006) 125505-1–4.
[11] P.A. Anderson, C.H. Swartz, D. Carder, R.J. Reeves, S.M. Durbin, S. Chandril, T.H. Myers, Buried p-type layers in Mg-doped InN, Appl. Phys. Lett. 89 (2006) 184104-1–3.

[12] J.W. Ager III, N. Miller, R.E. Jones, K.M. Yu, J. Wu, W.J. Schaff, W. Walukiewicz, Mg-doped InN and InGaN–photoluminescence, capacitance-voltage and thermopower measurements, phys. stat. sol. (b) 245 (2008) 873–877.
[13] W. Walukiewicz, Intrinsic limitations to the doping of wide-gap semiconductors, Physics B 302 (2001) 123–134.
[14] S.X. Li, K.M. Yu, J. Wu, R.E. Jones, W. Walukiewicz, J. Ager III, W. Shan, E.E. Haller, H. Lu, W.J. Schaff, Fermi-level stabalization energy in group III nitrides, Phys. Rev. B 71 (2005) 161201-1–4.
[15] G.F. Brown, J.W. Ager III, W. Walukiewicz, W.J. Schaff, J. Wu, Probing and modulating surface electron accumulation in InN by the electrolyte gated Hall effect, Appl. Phys. Lett. 93 (2008) 262105-1–3.
[16] P.D.C. King, T.D. Veal, P.H. Jefferson, C.F. McConville, H. Lu, W.J. Schaff, Phys. Rev. B 75 (2007) 115312-1–7.
[17] O. Jani, B. Jampana, M. Mehta, H. Yu, I. Ferguson, R. Opila, C. Honsberg, Optimization of GaN window layer for InGaN solar cells using polarization effect, in: 33rd IEEE Photovoltaic Specialists Conference, San Diego, California, USA, 2008.
[18] S.D. Burnham, G. Namkoong, D.C. Look, B. Clafin, W.A. Doolitte, Reproducible increased Mg incorporation and large hole concentration in GaN using metal modulated epitaxy, J. Appl. Phys. 104 (2008) 024902-1–5.
[19] E.F. Schubert, L.W. Tu, G.J. Zydzik, R.F. Kopf, A. Benvenuti, M.R. Pinto, Elimination of heterojunction band discontinuities by modulation doping, Appl. Phys. Lett. 60 (1992) 466–468.
[20] N. Miller, R.E. Jones, K.M. Yu, J.W. Ager, Z. Liliental-Weber, E.E. Haller, W. Walukiewicz, T.L. Williamson, M.A. Hoffbauer, Low-temperature grown compositionally graded InGaN films, phys. stat. sol. (c) **5** (2008) 1866–1869.
[21] G. Sassi, Theoretical analysis of solar cells based on graded band-gap structures, J. Appl. Phys. 54 (1983) 5421–5427.
[22] G.F. Virshup, C.W. Ford, J.G. Werthen, A 19% efficient AlGaAs solar cell with graded band gap, Appl. Phys. Lett. 47 (1985) 1319–1321.
[23] M. Gloeckler, J.R. Sites, Band-gap grading in Cu(In,Ga)Se2 solar cells, J. Phys. Chem. Solids 66 (2005) 1891–1894.
[24] M.E. Levinshtein, S.L. Rumyantsev, M.S. Shur, in: Properties of Advanced Semiconductor Materials: GaN, AlN, InN, BN, SiC, SiGe, John Wiley & Sons, New York, 2001.
[25] T. Inushima, M. Higashiwaki, T. Matsui, Optical properties of Si-doped InN grown on sapphire (0001), Phys. Rev. B 68 (2003) 235204-1–7.
[26] S.P. Fu, Y.F. Chen, Effective mass of InN epilayers, Appl.Phys. Lett. 85 (2004) 1523–1525.
[27] B. Santic, On the hole effective mass and free holes statistics in wurtzite GaN, Semicond. Sci. Technol. 18 (2003) 219–224.
[28] J. Wu, W. Walukiewicz, Band gaps of InN and group III nitride alloys, Superlattice. Microst. 34 (2003) 63–75.
[29] T.T. Mnatsakanov, M.E. Levinshtein, L.I. Pmortseva, S.N. Yurkov, G.S. Simin, M.A. Khan, Carrier mobility model for GaN, Solid-State Electron. 47 (2003) 111–115.
[30] L. Hsu, R.E. Jones, S.X. Li, K.M. Yu, W. Walukiewicz, Electron mobility in InN and III-N alloys, J. Appl. Phys. 102 (2007) 073705-1–6.
[31] Z.Z. Bandic, P.M. Bridger, E.C. Piquette, T.C. McGill, Minority carrier diffusion length and lifetime in GaN, Appl. Phys. Lett. 72 (1998) 3166–3168.
[32] F. Chen, A.N. Cartwright, H. Lu, W.J. Schaff, Temperature dependence of carrier lifetimes in InN, Appl. Phys. Lett. 87 (2005) 212104-1–3.
[33] J.F. Muth, J.H. Lee, I.K. Shmagin, R.M. Kolbas, H.C. Caser, B.P. Keller, U.K. Mishra, S.P. DenBaars, Absorption coefficient, energy gap, exciton binding energy, and recombination lifetime of GaN obtained from transmission measurements, Appl. Phys. Lett. 71 (1997) 2572–2574.
[34] F. Bernardini, V. Fiorentini, D. Vanderbilt, Spontaneous polarization and piezoelectric constants of III–V nitrides, Phys. Rev. B 56 (1997) R10024–R10027.
[35] C.F. Shih, N.C. Chen, P.H. Chang, K.S. Liu, Band offsets of InN/GaN interface, Japan. J. Appl. Phys. 44 (2005) 7892–7895.
[36] G. Martin, A. Botchkarev, A. Rockett, H. Morkoc, Valence-band discontinuties of wurtzite GaN, AlN, and InN heterojunctions measured by x-ray photoemission spectroscopy, Appl. Phys. Lett. 68 (1996) 2541–2543.
[37] M.A. Green, K. Emery, Y. Hishikawa, W. Warta, Solar Cell Efficiency Tables (Version 32), Prog. Photovolt: Res. Appl. 16 (2008) 61–67.
[38] T. Takamoto, E. Ikeda, H. Kurita, M. Ohmori, Over 30% efficient InGaP/GaAs tandem solar cells, Appl. Phys. Lett. 70 (1997) 381–383.
[39] S. Nakamura, The Roles of Structural Imperfections in InGaN-Based Blue Light-Emitting Diodes and Laser Diodes, Science 281 (1998) 956–961.